

Cluster Detection Capabilities of the Average Nearest Neighbor Ratio and Ripley's K Function on Areal Data: an Empirical Assessment

Nadeesha Vidanapathirana¹, Yuan Wang¹, Alexander C. McLain¹, Stella Self¹

¹Department of Biostatistics and Epidemiology, University of South Carolina, Columbia, SC.

Spatial clustering detection methods are widely used in many fields of research including epidemiology, ecology, biology, physics, and sociology. In these fields, areal data is often of interest; such data may result from spatial aggregation (e.g. the number disease cases in a county) or may be inherent attributes of the areal unit as a whole (e.g. the habitat suitability of conserved land parcel). This study aims to assess the performance of two spatial clustering detection methods on areal data: the average nearest neighbor (ANN) ratio and Ripley's K function. These methods are designed for point process data, but their ease of implementation in GIS software and the lack of analogous methods for areal data have contributed to their use for areal data. Despite the popularity of applying these methods to areal data, little research has explored their properties in the areal data context. In this paper we conduct a simulation study to evaluate the performance of each method for areal data under different types of spatial dependence and different areal structures. The results shows that the empirical type I error rates are inflated for the ANN ratio and Ripley's K function, rendering the methods unreliable for areal data.

Introduction

Researchers have been using spatial clustering analysis for many years to analyze data for spatial patterns. One of the earliest examples of spatial clustering analysis in public health occurred in 1894 when Dr. John Snow mapped the location of cholera cases to identify the source of an outbreak in London (Moore & Carpenter, 1999). Over the past few decades, the popularization of

geographical information systems (GIS) software has fueled the development and use of many new methods of spatial analysis. A Google Scholar search for ‘spatial clustering’ returns 15,600 results dated between 2001 and 2010, with an increase to 28,000 results between 2011 and 2020. Both point process (latitude-longitude) and areal data can exhibit spatial patterns, and a variety of methods have been developed to analyze spatial patterns in both types of data.

One of the oldest spatial clustering techniques is the average nearest neighbor (ANN) ratio, which was developed as a statistical test for spatial clustering (Clark & Evans, 1954). This method computes the distance between each observation location and its nearest neighbor, and the average ‘nearest neighbor distance’ (where the average is taken over all locations of observed data) is used to compute a test statistic. The ANN ratio has been widely used to detect clustering in various types of point process data, including clustering of disease cases (Aziz et al., 2012; Khademi et al., 2016; Melyantono, Susetya, Widayani, Tenaya, & Hartawan, 2021), crime hotspots (Brookman-Amisshah, Wemegah, & Okyere, 2014; Wing & Tynon, 2006; Z. Zhang et al., 2020) and clustering of archeological artifacts (Kıroğlu, 2003; Whallon, 1974). The ANN ratio has also been used to detect clustering in areal data (after mapping to centroids) in disease case data (Mollalo, Alimohammadi, Shirzadi, & Malek, 2015) aggregated to the municipality level.

Ripley’s K function was first developed in 1976 and can describe spatial patterns at different scales simultaneously. For a given distance t , Ripley’s K function returns the expected number of observation locations within a distance of t from a randomly selected observation location. Given a study area, a researcher can use Ripley’s K function to determine if observation locations are clustered, dispersed, or randomly distributed throughout the study area. Ripley’s K function has been applied to point process data for a variety of purposes including detecting disease clusters (Hohl, Delmelle, Tang, & Casas, 2016; Lentz, Blackburn, & Curtis, 2011; Ramis et al., 2015),

analyzing the spatial distribution patterns of plant communities (Haase, 1995; Moeur, 1993; Wolf, 2005), and detecting crime hotspots (Lu & Chen, 2007; Vadlamani & Hashemi, 2020). It has also been applied to areal data (after mapping the areal units to their centroids) in a variety of applications including disease case data aggregated at the municipality level (Karunaweera et al., 2020; Mollalo et al., 2015; Skog, Linde, Palmgren, Hauska, & Elgh, 2014), locations of conserved land (Zipp, Lewis, & Provencher, 2017), locations of land parcels in industrial use (Qiao, Huang, & Tian, 2019), human-wildlife interactions (Kretser, Sullivan, & Knuth, 2008), and rockfall events (Tonini & Abellan, 2014).

The ANN ratio and Ripley's K function were developed for point process data. However, Environmental Systems Research Institute (ESRI) ArcGIS software allows the user to implement both these methods on areal data using the average nearest neighbors tool (ANN ratio) and the multidistance spatial cluster analysis tool (Ripley's K function); both tools are in the spatial statistics toolbox. When the user applies either method to areal data (i.e. polygon features), ArcGIS automatically maps each polygon feature to its centroid and applies the method to the resulting set of points (Esri, 2021a; Esri, 2021b). To our knowledge, the performance of the ANN ratio and Ripley's K function under such circumstances has never been evaluated. Both methods assume under the null hypothesis that the observation locations arise from a homogenous point process. However, for areal data the centroids of smaller units will inherently be closer to the centroids of their neighbors when compared to the centroids of larger units, and thus unless all the units are the same size it is impossible for their centroids to arise from a homogeneous Poisson process. As the homogeneous Poisson process assumption is violated for areal data, it is advisable to assess the performance (i.e. empirical type I error rate and empirical power) of the ANN ratio and Ripley's K function when applied to areal data. In this paper, we conduct a simulation study to evaluate

the performance of each method for areal data under different types of spatial dependence and three different areal structures. Section 2 presents the detailed description of the two spatial clustering methods. Section 3 describes the simulation study and its results. Section 4 provides some theoretical results and Section 5 contains concluding remarks.

Methods

The ANN ratio and Ripley's K function can be used to perform a hypothesis test for the presence of spatial clustering or dispersion. The null hypothesis for each of these tests is that the observed locations exhibit complete spatial randomness (CSR), that is, the observation locations arise from a two-dimensional homogeneous Poisson process. Formally, a stochastic process is said to be a homogeneous Poisson process with rate λ if the number of events in any bounded region A , denoted $N(A)$, is Poisson distributed with mean intensity $\lambda|A|$, that is, $\Pr(N(A) = n) = e^{-\lambda|A|}(\lambda|A|)^n/n!$, where $|A|$ denotes the area of A . Given that there are n events in A , those events form an independent random sample from a uniform distribution on A (Cressie, 1994).

Average Nearest Neighbor Ratio

The average nearest neighbor (ANN) ratio was initially developed to classify spatial patterns in plant populations (Clark & Evans, 1954). In this context, the observed data consists of locations of observed plants, measured as coordinates in two-dimensional space. This method quantifies the randomness (or lack thereof) among the observed point locations by measuring the distance from each point to its nearest neighbor and using these distances to compute the average nearest neighbor (ANN) ratio given by

$$R = \frac{\bar{r}_O}{\bar{r}_E} \quad (1)$$

where $\bar{r}_O = \frac{\sum_{i=1}^N r_i}{N}$, r_i denotes the distance from the i^{th} individual to its nearest neighbor, N denotes the total number of observations, $\bar{r}_E = \frac{1}{2\sqrt{\rho}}$ is the expected value of \bar{r}_O under CSR for an infinite study area, $\rho = \frac{N}{|A|}$ is the density of the observed distribution, and $|A|$ is the size of the study area.

Under CSR, $E(R) = 1$, and for a perfectly clustered distribution (i.e., all points fall at the same location), $E(R) = 0$. Values of R greater than 1 indicate that the points are distributed more uniformly than expected under CSR. To use the ANN ratio for hypothesis testing, it is assumed that the distribution of r_O under the null hypothesis of CSR is approximately normal. A z-score for the statistic is calculated by

$$z = \frac{\bar{r}_O - \bar{r}_E}{\sigma_{\bar{r}_E}}, \quad (2)$$

where $\sigma_{\bar{r}_E}$ is the standard error of the mean distance to the nearest neighbor under CSR. It can be shown that $\sigma_{\bar{r}_E} = \frac{0.26136}{\sqrt{N\rho}}$. A significantly negative z-score indicates clustering, and a significantly positive score indicates dispersion. See Figure 1 for examples of clustering, dispersion, and complete spatial randomness.

Clark and Evans (1954) note some limitations of their procedure, such as the sensitivity to the chosen study area and inability to distinguish between certain types of spatial dependence (e.g., tightly clustered points in one place vs pairs of points scattered in population). In this situation, they suggest an extension to this measure by constructing a circle for each observation with an infinite radius, dividing the circle into equal sectors, and measuring the distance from the individual to its nearest neighbor for each of the sectors. They also point out that problems may

arise when the data consist of large areal units rather than points and the centroid of each unit is used to calculate the ANN ratio (Clark & Evans, 1954).

Ripley' K Function

The ANN ratio discussed above is based on first-order statistics, i.e., the mean of the distances between observation locations. One of the limitations of the method is the inability to test point patterns at different scales simultaneously (Ripley, 1977). For example, it is possible for data to be clustered at a small scale and clustered at a larger scale (i.e., the clusters are clustered) or clustered at a small scale but dispersed at a large scale (i.e., the clusters occur at somewhat regular intervals). Ripley's K function is a second-order spatial analysis tool (i.e., uses variances of the distances between observations) that can address the issue of scale-dependent spatial patterns. Here we only consider Ripley's K function for univariate spatial patterns in two dimensions, but it can also be extended for multivariate spatial patterns (ex: comparing spatial patterns of two species) (Dixon, 2001). Let $n_t(s)$ denote the number of points within radius t at point s . The function K is given by

$$K(t) = \frac{E(n_t(s))}{\lambda},$$

where λ is the density (number of points per unit area) and can be estimated as $\hat{\lambda} = \frac{N}{|A|}$, N is the observed number of points and $|A|$ is the size of the study area. The expectation is taken over the point locations. If the points follow a homogenous Poisson process (i.e., exhibit CSR), then $K(t) = \pi t^2$ which is the area of a circle of radius t . An approximately unbiased estimator for $K(t)$ was proposed by Ripley (Dixon, 2001; Ripley, 1976):

$$\hat{K}(t) = \hat{\lambda}^{-1} \sum_i \sum_{j \neq i} w_{ij}^{-1} \frac{I(d_{ij} < t)}{N}, \quad (3)$$

where d_{ij} is the distance between the i^{th} and j^{th} points, $I(d_{ij} < t)$ is the indicator function with the value of 1 if $d_{ij} < t$ and 0 otherwise, and w_{ij}^{-1} is a weighting factor associated with locations i and j that corrects for edge effects. Correction for edge effects is required if any distance d_{ij} is greater than the distance between point i and the boundary. Because the points outside the boundary are not included in the calculation of $\hat{K}(t)$, edge effects can lead to a biased estimator of $K(t)$. Various authors have proposed different edge corrections, such as buffer zones (Stern, Ribic, & Schatz, 1986; Szwagrzyk, 1990) or toroidal edge corrections (Ripley, 1979; Upton & Fingleton, 1985). One of the most commonly used edge corrections assigns w_{ij} a value of 1 if the circle centered at point i which passes through point j is entirely inside the study area and assigns w_{ij} equal to the proportion of the circumference of the circle that falls in the study area otherwise (Dixon, 2001).

To test for CSR, the estimator $\hat{L}(t) = [\hat{K}(t)/\pi]^{1/2}$ is sometimes used in practice, and $E(\hat{L}(t)) = t$ under CSR (Ripley, 1979). If the observed value of $K(t)$ is larger than the expected value of $K(t)$ for a given distance, the distribution is more clustered than CSR at that distance. If the observed value of $K(t)$ is smaller than the expected value of $K(t)$, the distribution is more dispersed than the random distribution at that distance. See Figure 1 for examples of data exhibiting clustering, dispersion, and CSR. Usually, the distribution of $\hat{K}(t)$ under the null hypothesis of CSR is estimated via Monte Carlo simulations, and critical values from the simulated distribution are used to define a rejection region for hypothesis testing.

Computing Ripley's K function can be computationally expensive for large datasets, as the number of distances between each pair of points must be computed. If inference is required, these

computations must be repeated for each dataset generated in the Monte Carlo simulations. Several computationally efficient methods have been suggested for use on large datasets. Tang, Feng, and Jia (2015) develop a massively parallel algorithm which uses graphical processing units (GPUs) to compute Ripley's K function for large datasets. G. Zhang, Huang, Zhu, and Keel (2016) propose two methods for computing Ripley's K which combines cloud computing with pre-sorting and efficient storage to reduce computation time. Wang et al. (2020) develop a distributed computing algorithm to compute Ripley's K function for large spatial-temporal datasets using Apache Spark. In addition to these methods, a number of software packages exist which are suitable for computing Ripley's K on smaller datasets, including the Multi-distance Spatial Cluster Analysis Tool in ESRI Arcgis (Esri. (2021b)), the spatstat package in R (Baddeley & Turner, 2021), and the splancs package in R (Bivand et al., 2017).

Simulations

A simulation study was conducted to assess the performance the ANN ratio and Ripley's K function under different areal data scenarios. In this study, we consider three areal unit structures: structure A_1 is a 20×20 regular grid where the units are of the same size, structure A_2 is the United States (US) counties in the states of North Carolina, Tennessee, South Carolina, Georgia, Alabama, and Mississippi where the units (counties) are roughly the same size but irregularly shaped, and structure A_3 is the Canadian forward sortation areas (FSAs) in the provinces of Alberta, Saskatchewan, and Manitoba where the units have vastly different sizes. Areal structures A_1 , A_2 , and A_3 contain $n_1 = 400$, $n_2 = 549$, and $n_3 = 267$ areal units, respectively. Observed data consists of a subset of the areal units presumed to have some characteristic of interest (e.g. implementing a county mask mandate during the COVID-19 pandemic), and data generation

consists of selecting this subset of units. We generate data under CSR and under two different types of clustering for two sample sizes. For each scenario, 500 datasets are simulated.

Data is generated by selecting the observed units from among the n_a total units present in areal structure A_a . We consider two sample sizes for each areal structure: $N = \lfloor \frac{n_a}{10} \rfloor$ and $N = \lfloor \frac{n_a}{4} \rfloor$, and generate data under the null hypothesis of no spatial pattern (data generation mechanism (DGM) D_1) and under two alternative hypotheses: a single large cluster (DGM D_2) and multiple smaller clusters (DGM D_3). Under DGM D_1 , which corresponds to the null hypothesis, the observed units are selected via uniform sampling without replacement from among the n_a total units. Under DGM D_2 , which corresponds to the single cluster, units in a pre-selected region of the study area are sampled with 10 times higher probability than the units in the rest of the study area. The regions of higher probability are shown in grey in Figure 2. DGM D_3 , which corresponds to multiple clusters, is an iterative process. First, an areal unit is selected via uniform random sampling, and this unit is observed, along with units which are directly adjacent to it. Another areal unit is then be sampled without replacement from the remaining unobserved units and is observed along with all adjacent units. This process is continued until N units have been observed. Examples of data generated on each areal structure under DGMs D_1 , D_2 and D_3 are shown in Figures 3-5, respectively.

The ANN ratio is calculated by using the centroids of the observed units as the observation locations. As the ANN ratio is known to be sensitive to the choice of the study area (often referred to as the window), we consider two different methods for selecting the window: window 1 is the entire study area and window 2 is the smallest possible rectangle that encloses all the observed locations (note that window 2 is dependent on the observed data, while window 1 is not). For DGM D_1 we perform an $\alpha = 0.05$ level two-tailed test by rejecting the null hypothesis if the

absolute value of the z-score exceeds the 0.975 quantile of a standard normal distribution. For DGMs D_2 and D_3 , we perform a left-tailed test (indicative of clustering) by rejecting the null hypothesis if the z-score falls below the 0.05 quantile of a standard normal distribution.

Ripley's K function was also evaluated using the centroids of the observed units as the observation locations. For each areal structure, the performance of Ripley's K function was evaluated at a sequence of 5 radii, with the smallest radius equal to the twice the smallest distance between any two-unit centroids and the largest radius equal to one-quarter of the width of the study area. For each dataset, Ripley's K function is evaluated at each radius using the Kest function in R (Baddeley & Turner, 2005) with the correction input as "Ripley". The distribution of Ripley's K function at each radius is approximated with 1000 Monte Carlo simulations. For DGM D_1 we perform an $\alpha = 0.05$ level two-tailed test by rejecting the null hypothesis if the absolute value of the estimate exceeds the 0.975 quantile of the Monte Carlo samples. For DGMs D_2 and D_3 , we perform a right-tailed test (indicative of clustering) by rejecting the null hypothesis if the estimate exceeds the 0.95 quantile of the Monte Carlo samples.

We assess the performance of the ANN ratio and Ripley's K function via empirical type I error rate and empirical power. For simulations under the null hypothesis (D_1), we report the global empirical type I error rate for the ANN ratio and the empirical type I error rate at each radius for Ripley's K function. For simulations under alternative hypotheses (D_2 and D_3), we report the global empirical power for the ANN ratio and the empirical power at each radius for Ripley's K function.

Results

Table 1 summarizes the empirical type I error rate (i.e., empirical probability of rejecting the null hypothesis of CSR when units are generated under CSR) and empirical power (i.e., the empirical probability of rejecting the null hypothesis of CSR when units are clustered) of the ANN ratio. When using window 1, the empirical type I error rate for all three areal structures is greater than 0.05 and its highest (0.99) for the Canadian FSAs where the units are vastly different sizes. When the sample size increases, the empirical type I error of each areal structure also increases. Under the alternative hypothesis, the empirical power of detecting a single cluster is 1.00 for the FSAs which is greater than both the regular grid and the counties. When the sample size increases, the empirical power of detecting a single cluster decreases to 0 for the regular grid and the US counties. When using window 2, the empirical type I error rate is severely inflated for all scenarios except the US counties under the smaller sample size. Furthermore, while there are appreciable differences in the empirical type I error rate when using the different windows, there is no clear pattern of increase or decrease. The empirical power for window 2 is lower for all scenarios except the US counties under the larger sample size.

Table 2 summarizes the empirical type I error and the empirical power of Ripley's K function. The empirical type I error rate is far above its nominal level in almost all cases. For the US counties, the empirical power is high (close to 1) for all radii except the smallest radius R_1 . For the FSAs, the empirical power is 1.0 for all radii except for R_1 . In general, the empirical power for detecting clusters is high in all three areal structures under all radii except for the minimum radius R_1 under the US counties and CA FSAs.

Theoretical Results

It is possible to obtain an analytical expression for $K(t)$ when areal data is generated on an infinite regular grid with each unit being observed with probability p . For simplicity and without loss of

generality, we assume a distance of one unit between centroids of adjacent grid cells. We begin by counting the number of centroids within a distance of t of a fixed centroid, denoted $N(t)$. This problem is equivalent to the well-studied Gauss Circle Problem of counting the number of points on an integer lattice within a distance of t of the origin. It can be shown that

$$N(t) = 1 + 4 \sum_{i=0}^{\infty} \left(\lfloor \frac{t^2}{4i+1} \rfloor - \lfloor \frac{t^2}{4i+3} \rfloor \right).$$

It can further be shown that $N(t)$ is approximately equal to πt^2 where the error term $Er(t) = N(t) - \pi t^2$ is such that $|Er(t)| \leq Ct^\theta$, where $1/2 < \theta \leq 131/208$ (Hardy, 1915, 1999). Recalling that the units are observed with probability p , then we expect $pN(t)$ observed units within a distance of t . Note that our assumption that the distance between centroids is equal to one unit implies density of $\lambda = p$, and thus $K(t)_{grid} = N(t)$. Under the null distribution of CSR, we have the usual $K(t)_{CSR} = \pi t^2$. Therefore, there are infinitely many values of t such that

$$|K(t)_{grid} - K(t)_{CSR}| = |N(t) - \pi t^2| = |Er(t)| > Ct^{1/2}.$$

Therefore even as t becomes large, the distribution of $K(t)_{grid}$ is not well approximated by the distribution of $K(t)_{CSR}$.

Conclusion

This study aimed to evaluate the performance of the ANN ratio and Ripley's K function on areal data using an extensive simulation study. Three areal structures, three types of spatial patterns and two different sample sizes were considered. As previously mentioned, the ANN ratio and Ripley's K functions are intended for point process data but in practice these methods are often used for areal data by mapping each areal unit to its centroid. Our results show that the empirical type I

error rates of the ANN ratio and Ripley's K function are inflated for the simulated data regardless of the sample size. We also see that the ANN ratio gives different results depending on which window is used for the ANN ratio calculation. The highly inflated empirical type I error rate makes both these methods unreliable for detecting spatial clustering in areal data. In the case of Ripley's K function applied to a regular grid, the inflated empirical type I error rate observed in our simulation study is confirmed by the theoretical divergence of $K(t)_{grid}$ and $K(t)_{CSR}$.

These findings have important implications for the use of these methods on areal data. An inflated type I error rate implies a high false discovery rate, meaning that researchers who have applied these methods to areal data may have wrongly concluded that their data exhibited a spatial pattern. In epidemiology, this may manifest as the discovery of non-existent disease clusters or outbreaks. In ecology, this the misapplication of these methods may lead researcher to conclude that parcels of conserved land are clustering together to create larger, higher quality habitats, when in fact they are not. In civil engineering and urban planning, the use of these methods could cause researcher to conclude that parcels of land designated for certain uses (parking, recreation, open space, etc.) are well dispersed throughout an urban area when such is not the case. As ESRI Arcgis software automatically applies these methods to areal data by mapping units to their centroids, these results are particularly concerning for ESRI users. The development of spatial clustering detection methods which are better suited for areal data is an excellent area for future work. In the absence of such methods, clustering analysis should be applied only to point process data unless the reliability of these methods for a particular areal data application can be demonstrated via simulation studies.

Funding

SS and AM were partially supported by National Institutes of Health grant NIGMS P20GM130420.

References

- Aziz, S., Ngui, R., Lim, Y., Sholehah, I., Nur Farhana, J., Azizan, A., & Wan Yusoff, W. (2012). Spatial pattern of 2009 dengue distribution in Kuala Lumpur using GIS application. *Trop Biomed*, 29(1), 113-120.
- Baddeley, A., & Turner, R. (2005). Spatstat: an R package for analyzing spatial point patterns. *Journal of statistical software*, 12(1), 1-42.
- Baddeley, A., & Turner, R. (2021). Package 'spatstat'.
- Bivand, R., Rowlingson, B., Diggle, P., Petris, G., Eglen, S., & Bivand, M. R. (2017). Package 'splancs'. *R package version*, 2.01-40.
- Brookman-Amisshah, M., Wemegah, T. D., & Okyere, F. T. (2014). Crime mapping and analysis in the Dansoman police subdivision, Accra, Ghana—A geographic information systems approach. *Journal of Environment and Earth Science*, 14(20), 28-37.
- Clark, P. J., & Evans, F. C. (1954). Distance to nearest neighbor as a measure of spatial relationships in populations. *Ecology*, 35(4), 445-453.
- Cressie, N. (1994). Models for spatial processes. *Statistical Methods for Physical Science*, 28(93), 124.
- Dixon, P. M. (2001). Ripley's K function. *Encyclopedia of environmetrics*, 3, 1796.
- Haase, P. (1995). Spatial pattern analysis in ecology based on Ripley's K-function: Introduction and methods of edge correction. *Journal of vegetation science*, 6(4), 575-582.
- Hardy, G. H. (1915). On the expression of a number as the sum of two squares. *Quart. J. Math.*, 46, 263-283.
- Hardy, G. H. (1999). *Ramanujan: twelve lectures on subjects suggested by his life and work* (Vol. 136): American Mathematical Soc.
- Hohl, A., Delmelle, E., Tang, W., & Casas, I. (2016). Accelerating the discovery of space-time patterns of infectious diseases using parallel computing. *Spatial and spatio-temporal epidemiology*, 19, 10-20.

- Karunaweera, N. D., Ginige, S., Senanayake, S., Silva, H., Manamperi, N., Samaranayake, N., . . . Zhou, G. (2020). Spatial epidemiologic trends and hotspots of Leishmaniasis, Sri Lanka, 2001–2018. *Emerging infectious diseases*, 26(1), 1.
- Khademi, N., Reshadat, S., Zanganeh, A., Saeidi, S., Ghasemi, S., & Zakiei, A. (2016). Identifying HIV distribution pattern based on clustering test using GIS software, Kermanshah, Iran. *HIV & AIDS Review*, 15(4), 147-152.
- Kıroğlu, M. F. (2003). *A GIS based spatial data analysis in Knidian amphora workshops in Reşadiye*. Citeseer,
- Kretser, H. E., Sullivan, P. J., & Knuth, B. A. (2008). Housing density as an indicator of spatial patterns of reported human–wildlife interactions in Northern New York. *Landscape and Urban Planning*, 84(3-4), 282-292.
- Lentz, J. A., Blackburn, J. K., & Curtis, A. J. (2011). Evaluating patterns of a white-band disease (WBD) outbreak in *Acropora palmata* using spatial analysis: a comparison of transect and colony clustering. *PloS one*, 6(7), e21830.
- Lu, Y., & Chen, X. (2007). On the false alarm of planar K-function when analyzing urban crime distributed along streets. *Social science research*, 36(2), 611-632.
- Melyantono, S. E., Susetya, H., Widayani, P., Tenaya, I. W. M., & Hartawan, D. H. W. (2021). The rabies distribution pattern on dogs using average nearest neighbor analysis approach in the Karangasem District, Bali, Indonesia, in 2019. *Veterinary World*, 14(3), 614.
- Moeur, M. (1993). Characterizing spatial patterns of trees using stem-mapped data. *Forest science*, 39(4), 756-775.
- Mollalo, A., Alimohammadi, A., Shirzadi, M. R., & Malek, M. R. (2015). Geographic information system-based analysis of the spatial and spatio-temporal distribution of zoonotic cutaneous leishmaniasis in Golestan Province, north-east of Iran. *Zoonoses and public health*, 62(1), 18-28.
- Moore, D. A., & Carpenter, T. E. (1999). Spatial analytical methods and geographic information systems: use in health research and epidemiology. *Epidemiologic reviews*, 21(2), 143-161.

- Qiao, L., Huang, H., & Tian, Y. (2019). The identification and use efficiency evaluation of urban industrial land based on multi-source data. *Sustainability*, *11*(21), 6149.
- Ramis, R., Gomez-Barroso, D., Tamayo, I., Garcia-Perez, J., Morales, A., Pardo Romaguera, E., & Lopez-Abente, G. (2015). Spatial analysis of childhood cancer: a case/control study. *PloS one*, *10*(5), e0127273.
- Ripley, B. D. (1976). The second-order analysis of stationary point processes. *Journal of applied probability*, *13*(2), 255-266.
- Ripley, B. D. (1977). Modelling spatial patterns. *Journal of the Royal Statistical Society: Series B (Methodological)*, *39*(2), 172-192.
- Ripley, B. D. (1979). Tests of 'randomness' for spatial point patterns. *Journal of the Royal Statistical Society: Series B (Methodological)*, *41*(3), 368-374.
- Skog, L., Linde, A., Palmgren, H., Hauska, H., & Elgh, F. (2014). Spatiotemporal characteristics of pandemic influenza. *BMC infectious diseases*, *14*(1), 1-14.
- Sterner, R. W., Ribic, C. A., & Schatz, G. E. (1986). Testing for life historical changes in spatial patterns of four tropical tree species. *The Journal of Ecology*, 621-633.
- Szwagrzyk, J. (1990). Natural regeneration of forest related to the spatial structure of trees: a study of two forest communities in Western Carpathians, southern Poland. *Vegetatio*, *89*(1), 11-22.
- Tang, W., Feng, W., & Jia, M. (2015). Massively parallel spatial point pattern analysis: Ripley's K function accelerated using graphics processing units. *International Journal of Geographical Information Science*, *29*(3), 412-439.
- Tonini, M., & Abellan, A. (2014). Rockfall detection from terrestrial LiDAR point clouds: A clustering approach using R. *Journal of Spatial Information Science*(8), 95-110.
- Upton, G., & Fingleton, B. (1985). *Spatial data analysis by example. Volume 1: Point pattern and quantitative data*: John Wiley & Sons Ltd.

- Vadlamani, S., & Hashemi, M. (2020). *Studying the impact of streetlights on street crime rate using geostatistics*. Paper presented at the 2020 IEEE 21st International Conference on Information Reuse and Integration for Data Science (IRI).
- Wang, Y., Gui, Z., Wu, H., Peng, D., Wu, J., & Cui, Z. (2020). Optimizing and accelerating space–time Ripley’s K function based on Apache Spark for distributed spatiotemporal point pattern analysis. *Future Generation Computer Systems, 105*, 96-118.
- Whallon, R. (1974). Spatial analysis of occupation floors II: the application of nearest neighbor analysis. *American Antiquity, 39*(1), 16-34.
- Wing, M. G., & Tynon, J. (2006). Crime mapping and spatial analysis in national forests. *Journal of Forestry, 104*(6), 293-298.
- Wolf, A. (2005). Fifty year record of change in tree spatial patterns within a mixed deciduous forest. *Forest Ecology and management, 215*(1-3), 212-223.
- Zhang, G., Huang, Q., Zhu, A.-X., & Keel, J. H. (2016). Enabling point pattern analysis on spatial big data using cloud computing: optimizing and accelerating Ripley’s K function. *International Journal of Geographical Information Science, 30*(11), 2230-2252.
- Zhang, Z., Sha, D., Dong, B., Ruan, S., Qiu, A., Li, Y., . . . Yang, C. (2020). Spatiotemporal patterns and driving factors on crime changing during black lives matter protests. *ISPRS International Journal of Geo-Information, 9*(11), 640.
- Zipp, K. Y., Lewis, D. J., & Provencher, B. (2017). Does the conservation of land reduce development? An econometric-based landscape simulation with land market feedbacks. *Journal of Environmental Economics and Management, 81*, 19-37.

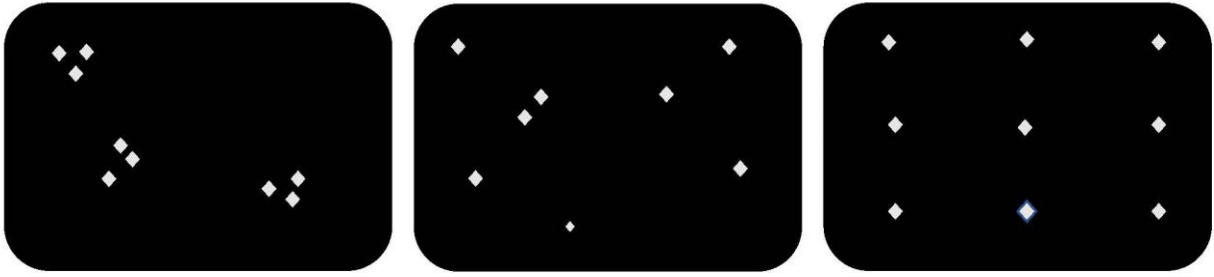


Figure 1. Examples of spatial patterns of clustering (left), CSR (middle), and dispersion (right).

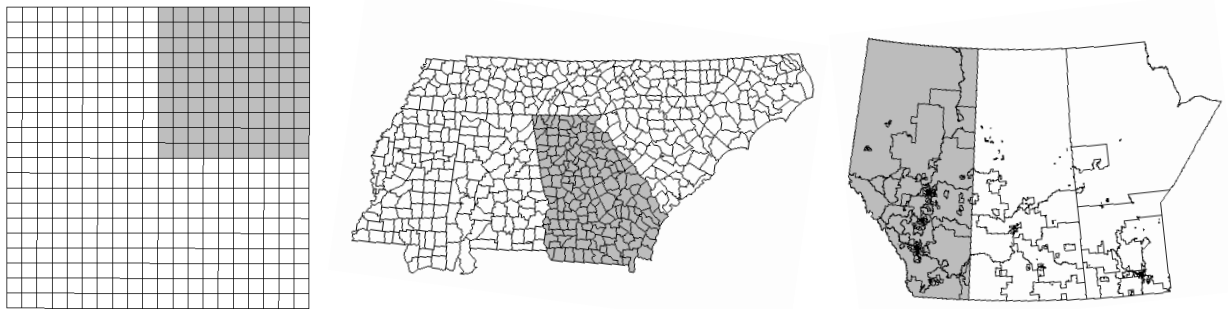


Figure 2. The regions of higher probability selected (grey) under single cluster (left 20x20 regular grid, middle USA counties in six states and right CA FSAs in three provinces).

Table 1. Empirical type I error and empirical power of the ANN ratio. $n_a = 400$ for regular grid, $n_a = 549$ for USA counties, $n_a = 267$ for Canadian FSAs.

DGM (Data generation mechanism)	Quantity	N	A ₁ : Regular Grid	A ₂ : US counties	A ₃ : Canadian FSAs
Window 1					
H_0 : CSR: D ₁	Empirical type I error	$\lfloor n_a/10 \rfloor$	1.00	0.99	1.00
		$\lfloor n_a/4 \rfloor$	0.39	0.35	0.99
H_a : Single Cluster: D ₂	Empirical power	$\lfloor n_a/10 \rfloor$	0.00	0.00	1.00
		$\lfloor n_a/4 \rfloor$	0.04	0.27	1.00
H_a : Multiple Clusters: D ₃	Empirical power	$\lfloor n_a/10 \rfloor$	0.00	0.95	1.00
		$\lfloor n_a/4 \rfloor$	1.00	1.00	1.00
Window 2					
H_0 : CSR: D ₁	Empirical type I error	$\lfloor n_a/10 \rfloor$	1.00	0.01	1.00
		$\lfloor n_a/4 \rfloor$	0.75	0.06	0.83
H_a : Single Cluster: D ₂	Empirical power	$\lfloor n_a/10 \rfloor$	0.00	0.36	1.00
		$\lfloor n_a/4 \rfloor$	0.00	0.24	0.76
H_a : Multiple Clusters: D ₃	Empirical power	$\lfloor n_a/10 \rfloor$	0.00	0.96	1.00
		$\lfloor n_a/4 \rfloor$	0.53	0.99	0.93

Table 2. Empirical type I error rate and empirical power of Ripley's K function.

Radius	Empirical type I error/ empirical power									
	R ₁		R ₂		R ₃		R ₄		R ₅	
N	$\lfloor \frac{n_a}{10} \rfloor$	$\lfloor \frac{n_a}{4} \rfloor$	$\lfloor \frac{n_a}{10} \rfloor$	$\lfloor \frac{n_a}{4} \rfloor$	$\lfloor \frac{n_a}{10} \rfloor$	$\lfloor \frac{n_a}{4} \rfloor$	$\lfloor \frac{n_a}{10} \rfloor$	$\lfloor \frac{n_a}{4} \rfloor$	$\lfloor \frac{n_a}{10} \rfloor$	$\lfloor \frac{n_a}{4} \rfloor$
DGM	The regular grid (A ₁)									
H ₀ : CSR: D ₁	0.98	1.00	0.92	1.00	0.84	0.78	0.75	0.49	0.90	1.00
H _a : Single cluster: D ₂	0.88	0.96	0.99	1.00	1.00	1.00	1.00	1.00	1.00	1.00
H _a : Multiple clusters: D ₃	1.00	1.00	1.00	1.00	1.00	1.00	1.00	0.99	1.00	0.79
	The US counties (A ₂)									
H ₀ : CSR: D ₁	0.98	1.00	0.85	0.62	0.85	0.64	0.77	0.73	0.79	0.71
H _a : Single cluster: D ₂	0.19	0.00	1.00	1.00	1.00	1.00	1.00	1.00	1.00	1.00
H _a : Multiple clusters: D ₃	0.35	0.00	1.00	1.00	1.00	1.00	1.00	0.98	0.94	0.91
	The Canadian FSAs (A ₃)									
H ₀ : CSR: D ₁	0.06	0.30	1.00	1.00	1.00	1.00	1.00	1.00	1.00	1.00
H _a : Single cluster: D ₂	0.08	0.38	1.00	1.00	1.00	1.00	1.00	1.00	1.00	1.00
H _a : Multiple clusters: D ₃	0.25	0.49	1.00	1.00	1.00	1.00	1.00	1.00	1.00	1.00